JOURNAL OF AIRCRAFT
Vol. 39, No. 4, July–August 2002

Separation Control in Duct Flows

Michael Amitay*
Georgia Tech Research Institute, Atlanta, Georgia 30332-0405
Dale Pitt†
The Boeing Corporation, St. Louis, Missouri 63134
and
Ari Glezer‡
Georgia Tech Research Institute, Atlanta, Georgia 30332-0405

Active control of separation in a duct flow is achieved using an array of fluidic actuators based on synthetic-jet technology. A two-dimensional serpentine duct model is designed to produce controlled separated flow in two configurations, in which the flow is either completely separated or has a separation bubble. An array of synthetic-jet actuators is placed within the separated flow domain in the diffuser section downstream of the onset of separation. Actuation leads to complete flow attachment up to $U_{in} = 75$ m/s ($M \approx 0.2$) and to partial reattachment up to $U_{in} = 105$ m/s ($M \approx 0.3$).

I. Introduction

ENGINE inlets, or air induction systems, have a major impact on the flight performance, mission effectiveness, and life-cycle cost of the air vehicles. As noted by Mayer and Anderson,[1] compact inlets/diffusers are developed to meet requirements for modern fighter/attack aircraft where signature considerations dictate a diffuser having a serpentine flow path to provide line-of-sight blockage of the engine face. These requirements have resulted in short, highly curved inlet diffusers (for example, Gridley and Cahill[2] and a McDonnell Douglas report[3]). A systems trade study[2] showed that a compact serpentine diffuser with a very aggressive offset (1.5 engine face diameters) in a relatively short length (3.1 engine face diameters), compared to conventional diffusers, lead to a 500-lb reduction in the vehicle empty weight and a 162-lb increase in fuel volume. However, the radical geometry changes in compact serpentine diffusers result in adverse internal pressure gradients and centrifugal forces that can lead to internal boundary-layer separation and therefore to lower total pressure recovery at the engine face. Presently, the separating boundary layer is one of the primary constraints in compact diffuser design.

Extensive work since the early 1980s has demonstrated that active manipulation of external separated shear flow over aerodynamic surface can result in complete or partial flow attachment. Active control approaches have employed both external[4] and internal[5] acoustic excitation, vibrating ribbons or flaps,[6] and steady and unsteady blowing/bleed[7] to manipulate the natural instabilities of the separating shear layer and achieve a Coanda-like flow attachment. These actuation approaches are limited by the relatively narrow frequency band to which the separating flow is receptive. The effectiveness of high-frequency broadband actuation was demonstrated by Smith et al.[8] and Amitay et al.,[9–11] who used fluidic actuation based on synthetic-jet technology to suppress flow separation. Although considerable attention has been devoted to the manipulation of external shear flows, little emphasis has been placed on separated flows within ducts, having complex geometries and sharp turns (for example, engine inlets). The control of these duct flows is further complicated by the presence of three-dimensional secondary flows. It appears that in common with separation control of external subsonic flows, where flow modifications are reflected in global changes in circulation and in turn the separation and reattachment dynamics, separation control in internal flows can affect changes in the global flow rate through the duct and thus in the structure of the separated flow. As just noted, separation control in propulsion/inlet systems is of specific interest because current designs that emphasize highly aggressive offset serpentine inlets and diffusers are prone to internal flow separation. The present paper reports an experimental investigation of the utility of a fluidic actuation based on synthetic-jet arrays to mitigate separation within a low-aspect-ratio duct model having prescribed internal changes in flow direction.

Received 16 February 2001; revision received 8 January 2002; accepted for publication 13 May 2002.

*Senior Research Engineer, Aerospace and Transportation Laboratory. Member AIAA.
†Associate Technical Fellow, Structures Department. Associate Fellow AIAA.
‡Professor, Woodruff School of Mechanical Engineering. Associate Fellow AIAA.

II. Experimental Setup

A. Duct Facility

The efficiency of synthetic-jet actuator arrays for the suppression of internal separation is investigated in a two-dimensional duct facility (Fig. 1) that was specifically designed to induce controlled separation. The inlet section of the rectangular (12.7×7.62 cm) duct is a 50-cm-long inlet and is followed by a variable cross-section duct having a hinged top surface that can be deflected at angles between $\beta = 0$ and 20 deg relative to the horizontal, as shown schematically in Fig. 1. The duct is connected to a high-pressure air system through a converging nozzle and a settling chamber, where freestream velocities up to $U_{in} = 105$ m/s ($M = 0.3$) can be realized. The magnitude of the adverse pressure gradient is set by the wall deflection, and, consequently, the location and the severity of the boundary-layer separation are controlled. The direction of the flow within the movable wall section can be altered by an internal wedge insert block as shown schematically in Fig. 1b. The test fixture is designed so that a synthetic-jet actuator block can be mounted either on the bottom wall (Fig. 1a) or on the top wall (Fig. 1b). The duct is also equipped with suction ports on all internal surfaces. When suction is applied on the upper surface, the flow remains attached to that surface and separates from the bottom surface as shown in Fig. 1a. It is well known that for these types of low-aspect-ratio ducts the separation is highly three-dimensional; therefore, in order to fix the streamwise and spanwise locations of the separation a spanwise trip is placed just upstream of the actuator block such that the actuator array is located within the separated flow domain. Two different trips having cross-stream heights of $c = 0.023 \cdot h$ and $0.042 \cdot h$ are used to

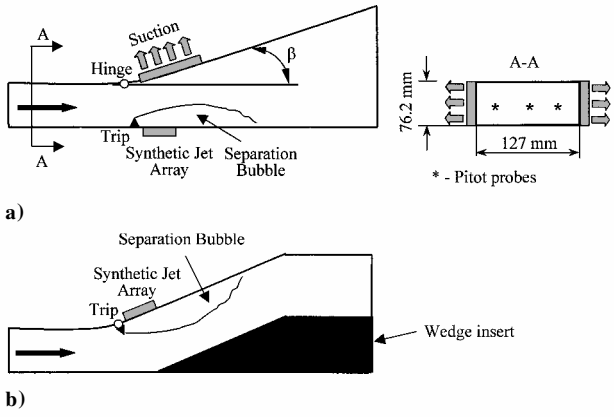

Fig. 1 Two-dimensional diffuser setup.

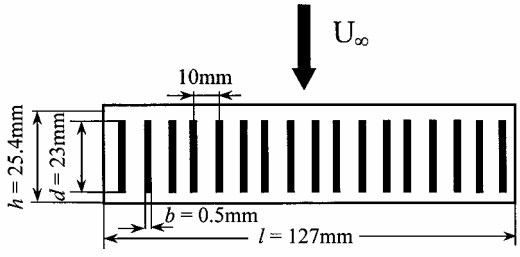

Fig. 2 Actuator array configuration.

control the streamwise extent of the separated region. Cross-stream distributions of the streamwise velocity are measured at three spanwise locations (5.08 cm apart) using a rake of three miniature (1 mm) total pressure tubes, where the center tube is aligned with the center of the duct. Pressure transducers (Druck Model PDCR22 and Scanivalve Model TDCR33D-1) having a range of 1 psi are used to measure the pressure to within ±0.004 psi.

B. Synthetic-Jet Array

An array of individually addressable actuators (Fig. 2) was designed to control spanwise nonuniform separation by using spanwise-variable actuation amplitude and time-dependent modulation of the actuation waveform. In the experiments reported here the jet velocity of each of the actuators was adjusted to produce spanwise-uniform actuation. The array is comprised of stacks of 17 individual actuator elements, which are assembled into a single block. The rectangular (0.5 × 23 mm) orifices are aligned with the flow direction and are 10 mm apart. Each block is installed within the duct wall so that the exit plane of the actuators jets is flush with the diffuser wall. The actuator array is calibrated in the absence of a crossflow using a miniature single wire (5 μm, 1 mm long) with an uncertainty of ±1%. The actuator performance is measured using the momentum coefficient C_μ, which is the ratio of the actuator jets' momentum flux to the freestream momentum flux (see Ref. 11). In the present work the jet velocity is 11 m/s, and the driving frequency is 1032 Hz.

Particle image velocimetry (PIV) is used to determine the degree of interaction between adjacent jets. The measurements are performed in a glass enclosure; the flow is seeded using incense smoke and is illuminated using a double-pulse ND-YAG laser. Image pairs are captured using a 1008 × 1016 pixel charge-coupled device camera with a magnification of 20 μm/pixel. Velocity vectors are computed on a 62 × 62 element grid using a standard cross-correlation algorithm and averaged over 300 realizations. The uncertainties of the computed velocity and spanwise vorticity are estimated to be ±3 and ±5%, respectively.

III. Results and Discussion

A. Synthetic-Jet Array

Some features of the flowfield of the jet array in the absence of a crossflow are investigated in a plane that includes the centerlines

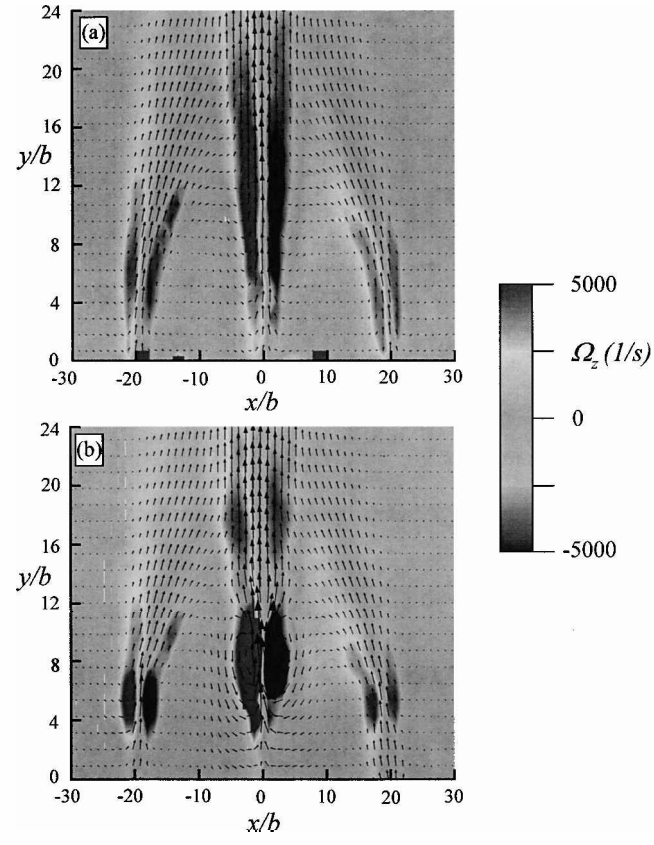

Fig. 3 Superposed velocity and vorticity fields in the center plane of the actuator array: a) time- and b) phase-averaged fields. Only the middle jet is activated.

of adjacent actuators using PIV. Images of the time- and phase-averaged velocity and vorticity distributions in the flowfield of a single jet are shown in Figs. 3a and 3b, respectively. These data show the formation of a weak jet on each side of the center (active) jet, presumably owing to unsteady pressure field that is induced in the vicinity of the orifice of the active jet. As shown in the PIV images, the weak jets merge with the center jet around $y/b \sim 18$. Cross-stream distributions of the streamwise velocity at $y/b = 6$ and 20 are extracted from the PIV data and are shown in Figs. 4a and 4b, respectively. Near the jet-exit plane (Fig. 4a) the velocity distribution has three distinct peaks, corresponding to the three jets in Fig. 3; however, the center (active) jet is substantially stronger than the induced side jets. Farther downstream at $y/b = 20$ (Fig. 4b), the three jets are merged, and the velocity distribution shows no remnants of the individual jets.

Similar to Figs. 3a and 3b, Figs. 5a and 5b show time- and phase-averaged distributions of velocity and vorticity fields, respectively, of a group of three active adjacent jets. It is remarkable that even when the left and right jets are active they are symmetrically tilted towards the center jet. As might be expected, this interaction is substantially diminished when additional jets are activated on the left and right, and the tilting is mostly experienced by the jets on the edges of the array. The phase-averaged vorticity map (Fig. 5b) shows that as a result of the interaction the vortex pair of the center jet leads in phase relative to the corresponding pairs of the right and left jets. The preceding vortex pairs of the side jets farther downstream are slightly distorted, and owing to the velocity induced by the center jet the inner vortex of each pair appears to be advected faster than the opposite vortex. These interactions are also evident in the cross-stream distributions of the time-averaged streamwise velocity in Figs. 6a and 6b. These distributions indicate that the strength of the jets is not identical and show monotonic increase in the magnitude of the centerline velocity from left to right. Unlike the data in Fig. 4b, the velocity distribution at $y/b = 20$ (Fig. 6b) still exhibits three distinct peaks.

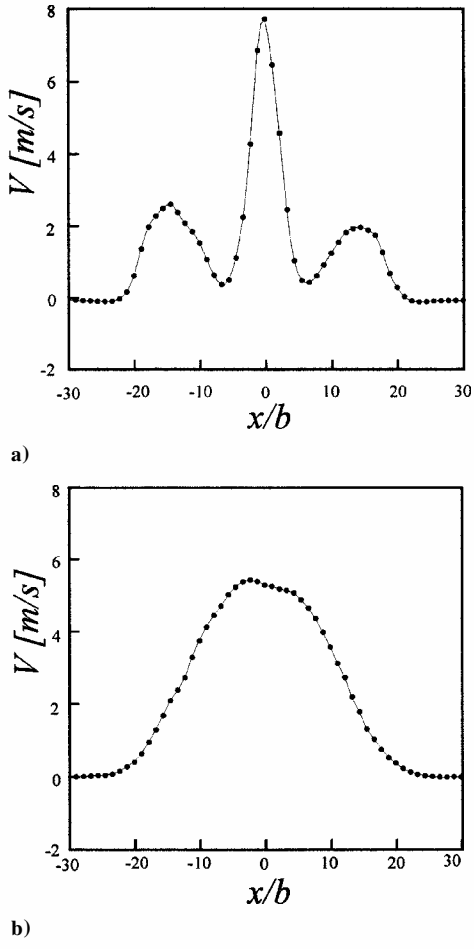

Fig. 4 Streamwise velocity distributions across the actuator array at a) $y/b = 6$ and b) $y/b = 20$. Only the center jet is active.

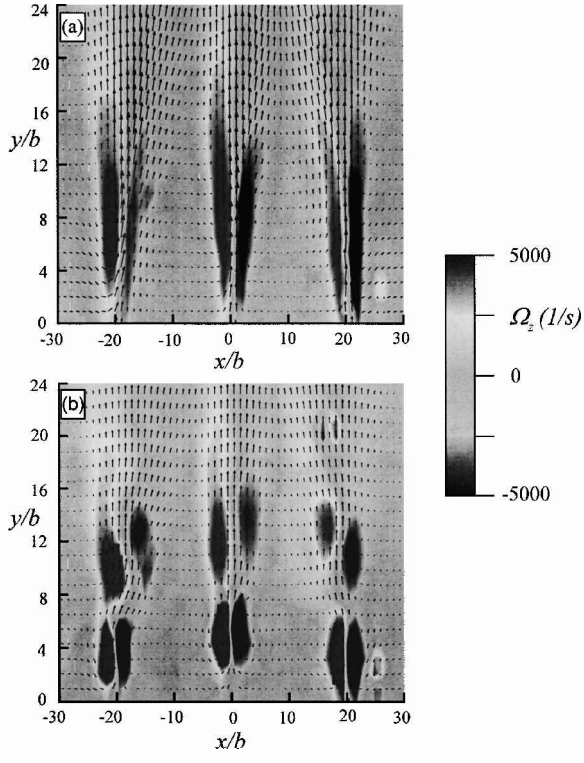

Fig. 5 Superposed velocity and vorticity fields in the center plane of the actuator array: a) time- and b) phase-averaged fields. All three jets are activated.

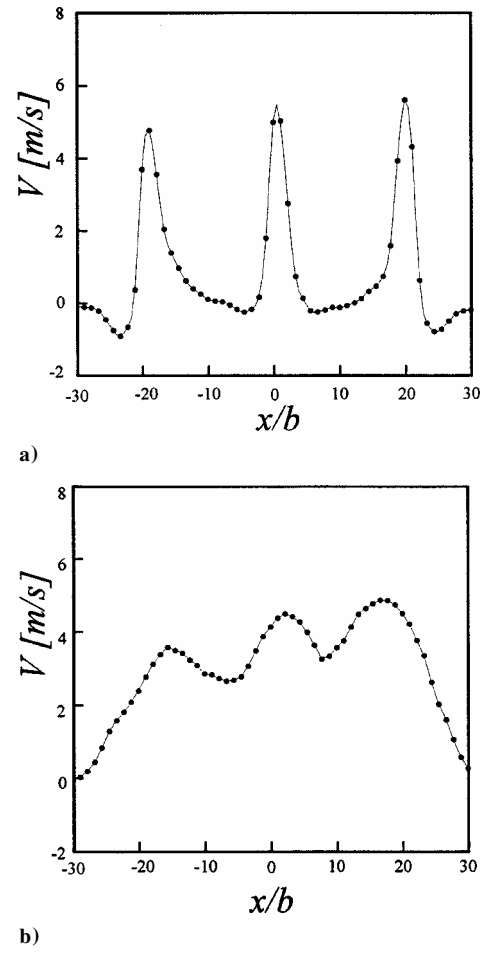

Fig. 6 Streamwise velocity distributions across the actuator array at a) $y/b = 6$ and b) $y/b = 20$. All three jets are active.

B. Two-Dimensional Duct

The effectiveness of the synthetic-jet actuators array is tested in the two duct configurations shown in Figs. 1a and 1b. In configuration a (Fig. 1a) the angle of the upper surface in the diffuser section is set at 14 deg, and suction is used to maintain attached flow on that surface. (In the absence of suction, the flow separates from this surface.)

Cross-stream distributions of the streamwise velocity measured near the bottom surface of the duct at three streamwise stations ($x/h = 0.17$, 0.5, and 0.67) are shown in Figs. 7a–7c. Nominally two-dimensional separation is induced at $x = 0$ by a spanwise trip having a characteristic height $c = 0.023 \cdot h$ (cf. Sec. II.A). In each figure velocity distributions at three spanwise positions are shown in the presence and absence of actuation. The freestream velocity in the upstream, fixed area, duct is 61 m/s ($M = 0.18$); the jet array (Fig. 2) is located just downstream of the trip and has a momentum coefficient of $C_\mu = 2 \times 10^{-3}$ per jet.

As shown in Fig. 7a, the cross-stream height of the separated domain is $y_s = 0.08 \cdot h$ above the bottom surface, and the velocity distributions at the three spanwise positions suggest that the separation is reasonably two-dimensional. The height of the separated domain is determined by the detection of flow reversal near the surface. When the jets are activated (as represented by the solid symbols), the cross-stream extent of the separated region is reduced to $y_s = 0.01 \cdot h$ on the duct centerline and to $y_s = 0.035 \cdot h$ off the centerline, indicating that the effect of actuation diminishes somewhat near the side walls of the duct presumably owing to the interaction of the separated flow region with the corners. Because the mass flow rate through the entire duct is fixed, the velocity near the duct centerline decreases when the flow is attached.

Farther downstream, at $x/h = 0.5$ (Fig. 7b) the height of the separated domain of the baseline flow is reduced from $y_s = 0.09 \cdot h$

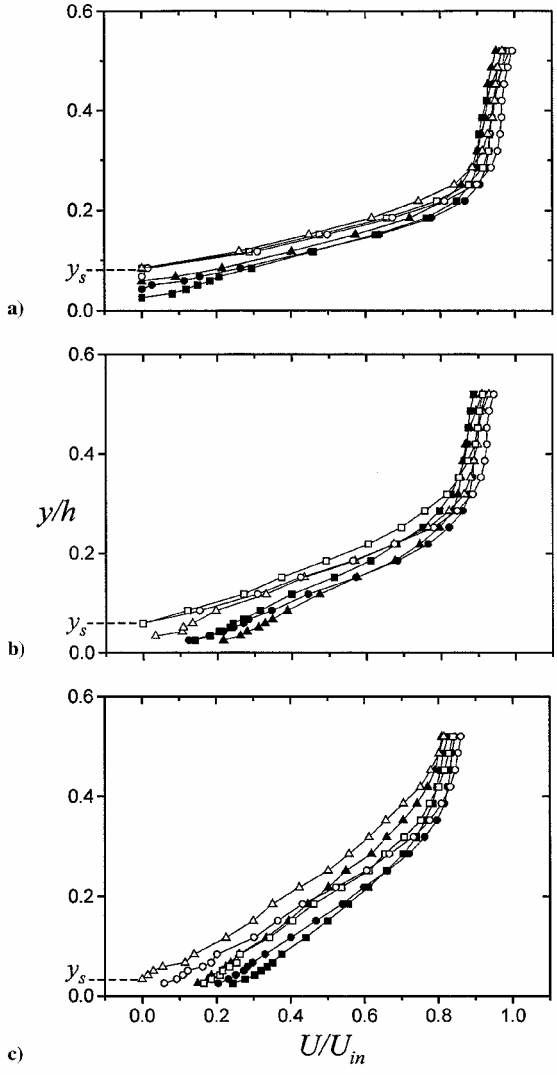

Fig. 7 Cross-stream distributions of the streamwise velocity at $M = 0.18$ for duct configuration a: a) $x/h = 0.17$, b) $x/h = 0.5$, and c) $x/h = 0.67$. Center probe: ■, actuated and □, baseline. Left probe: ●, actuated and ○, baseline. Right probe: ▲, actuated and △, baseline.

to $0.05 \cdot h$. Even though at this station the separation is no longer two-dimensional, the actuated flow is completely reattached across the entire span, as is evident from the magnitude of the streamwise velocity near the bottom wall. Finally, at $x/h = 0.67$ (Fig. 7c) the baseline flow is attached on the duct centerline and on the left side, and the height of the separated domain on the right side is $y_s = 0.02 \cdot h$. Actuation results in a complete reattachment. As in Fig. 7a, streamwise velocity of the attached flow near the wall in Figs. 7b and 7c increases significantly compared to the baseline flow, indicating a significant decrease in losses within the duct.

Velocity distributions within a serpentine-like duct configuration (configuration b, Fig. 1b), in which the upper and lower surfaces are parallel, are shown in Figs. 8a and 8b (measured at $x/h = 0.5$ and 0.67 downstream of the trip, respectively). For these measurements $U_{\text{in}} = 41$ m/s ($M = 0.12$), the characteristic height of the trip used to induce a two-dimensional separation is $c/h = 0.023$, and the cross-stream height of the separated domain in the baseline flow ($x/h = 0.5$, Fig. 8a) is $y_s = 0.05 \cdot h$. When actuation is applied downstream of the trip, the flow reattaches completely. However, the higher streamwise velocity at center span suggests that the flow on the centerline becomes attached closer to the trip than on the two sides. At $x/h = 0.67$ (Fig. 8b) the baseline flow is attached, but the actuated flow near the surface is somewhat faster than the baseline flow and becomes somewhat more spanwise uniform compared to the upstream station (Fig. 8a). The higher velocities near the wall suggest that, similar to configuration a, the actuation results

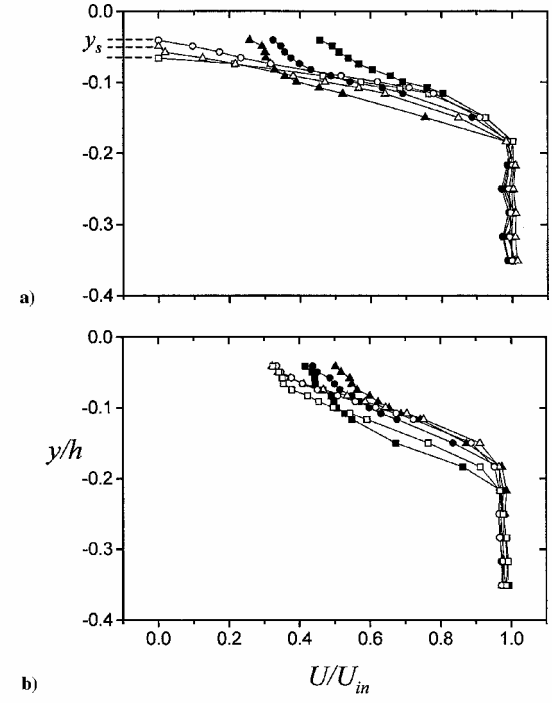

Fig. 8 Cross-stream distributions of the streamwise velocity at $M = 0.12$ for duct configuration b: a) $x/h = 0.5$ and b) $x/h = 0.67$. Trip height is $c/h = 0.023$. Symbols as in Fig. 7.

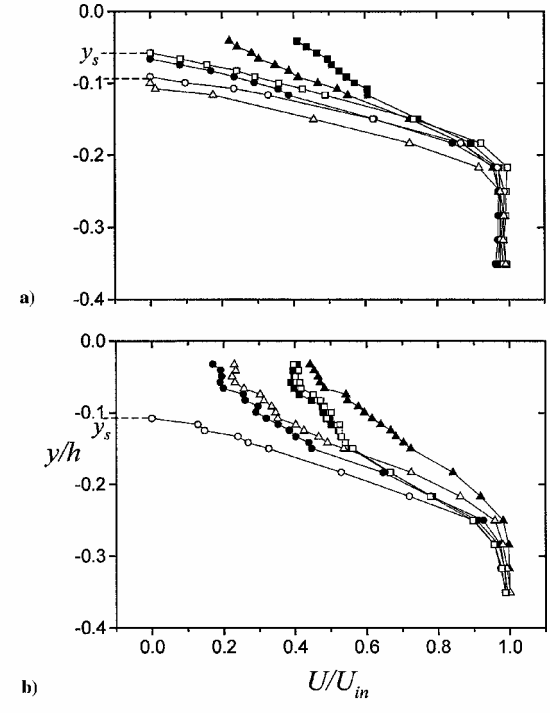

Fig. 9 Cross-stream distributions of the streamwise velocity at $M = 0.12$ for duct configuration b: a) $x/h = 0.5$ and b) $x/h = 0.67$. Trip height is $c/h = 0.042$. Symbols as in Fig. 7.

in reduced losses within the duct and can increase the volume flow rate.

To demonstrate the effects of the actuation on larger separated regions, a higher trip ($c/h = 0.042$) is used to increase the size of the separation bubble, resulting in a nonuniform (and asymmetric) separation domain (Fig. 9a). Farther downstream ($x/h = 0.67$, Fig. 9b) the flow is attached on the centerline as well as on the right side. However, in this case the flow is still separated on the left side of the duct. In the presence of actuation (represented by the solid symbols), there is a partial flow reattachment at the first downstream

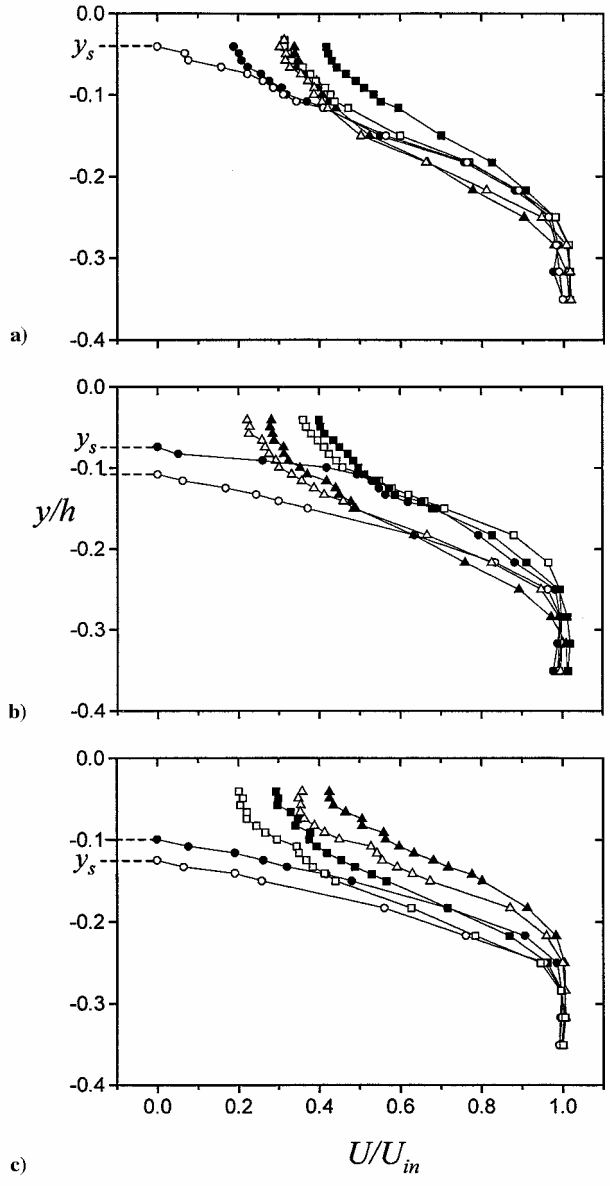

Fig. 10 Cross-stream distributions of the streamwise velocity at $x/h = 0.67$ for duct configuration b: a) $M = 0.18$, $C_\mu = 2.01 \times 10^{-3}$; b) $M = 0.23$, $C_\mu = 1.2 \times 10^{-3}$; and c) $M = 0.3$, $C_\mu = 7.2 \times 10^{-4}$. Trip height is $c/h = 0.042$. Symbols as in Fig. 7.

measurement station ($x/h = 0.5$, Fig. 9a). Farther downstream at $x/h = 0.67$ (Fig. 9b), the actuation yields a complete flow reattachment across the span (although the reattachment is not two-dimensional), suggesting that actuation leads to a significant reduction in the size of the separation bubble.

The effectiveness of the jets is also investigated at higher Mach numbers $M = 0.18$, 0.23, and 0.3 as shown in Figs. 10a, 10b, and 10c, respectively. The corresponding momentum coefficients of the actuator jets (for a fixed jet velocity) decrease to 2.1×10^{-3}, 1.2×10^{-3}, and 7.2×10^{-4}. Increasing the Mach number increases the cross-stream extent of the separation on the left side of the duct (open circles) and slightly decreases the streamwise velocity near the wall on the centerline and on the left side of the duct. These data also show that although the effectiveness of the actuators diminishes with C_μ the actuation still results in a significant reduction in the extent of the separation bubble. These results suggest that a further increase in the magnitude of the momentum coefficient of the jets can yield complete or partial flow reattachment even at higher Mach numbers.

IV. Conclusions

Separation control using fluidic actuation based on synthetic (zero mass flux) jets that was used before in external flows is demonstrated in internal duct flow. A two-dimensional serpentine duct model is designed to produce controlled partial or complete internal separation in two configurations. In the first configuration the hinged (upper) diffuser wall is open to 14 deg, and suction is used to maintain attached flow on that surface, resulting in a separation bubble on the opposite (bottom) surface. The second configuration is a serpentine duct (configuration b) in which the flow surfaces are parallel, and a separation bubble forms on the expanding surface. In both configurations a trip is used to effect a nominally two-dimensional separation across the width of the duct. The jet array is placed downstream of separation (that is, within the separated flow domain). Actuation results in a significant reduction in the streamwise extent of the separation flow domain. For $M < 0.2$ the flow is completely attached, and $0.2 < M < 0.3$ reattachment is detected farther upstream than in the baseline flow. Flow reattachment results in reduced losses within the duct and can increase the volume flow rate.

In the present work the momentum coefficient of the jets within the array varies between 7×10^{-4} and 2×10^{-3}. (The strength of the jets is spanwise uniform.) The present data suggest that an increase in the jet strength and the application of spanwise uniform actuation can result in a more effective control of internal separation.

Acknowledgments

This work was supported in part by Defense Advanced Research Projects Agency and monitored by Ephraim Garcia. The authors would like to acknowledge a number of useful discussions with D. E. Parekh and V. Kibens during the experiments.

References

[1] Mayer, D. W., and Anderson, B. H., "3D Subsonic Diffuser Design and Analysis," AIAA Paper 98-3418, July 1998.

[2] Gridley, M. C., and Cahill, M. J., "ACIS Air Induction System Trade Study," AIAA Paper 96-2646, July 1996.

[3] McDonnell Douglas Corp., "Advanced Compact Inlet Systems Air Induction System Trade Study Final Report," MDC 96P0002, Sponsored by Air Force Research Lab., Jan. 1996.

[4] Ahuja, K. K., and Burrin, R. H., "Control of Flow Separation by Sound," AIAA Paper 84-2298, Jan. 1984.

[5] Huang, L. S., Maestrello, L., and Bryant, T. D., "Separation Control over an Airfoil at High Angles of Attack by Sound Emanating from the Surface," AIAA Paper 87-1261, Jan. 1987.

[6] Neuburger, D., and Wygnanski, I., "The Use of a Vibrating Ribbon to Delay Separation on Two Dimensional Airfoils," TR-88-0004, 1987.

[7] Seifert, A., Darabi, A., and Wygnanski, I., "Delay of Airfoil Stall by Periodic Excitation," *Journal of Aircraft*, Vol. 33, No. 4, 1996, pp. 691–698.

[8] Smith, D. R., Amitay, M., Kibens, K., Parekh, D. E., and Glezer, A., "Modification of Lifting Body Aerodynamics Using Synthetic Jet Actuators," AIAA Paper 98-0209, Jan. 1998.

[9] Amitay, M., Smith, B. L., and Glezer, A., "Aerodynamic Flow Control Using Synthetic Jet Technology," AIAA Paper 98-0208, Jan. 1998.

[10] Amitay, M., Kibens, V., Parekh, D. E., and Glezer, A., "Flow Reattachment Dynamics over a Thick Airfoil Controlled by Synthetic Jet Actuators," AIAA Paper 99-1001, Jan. 1999.

[11] Amitay, M., Smith, D. R., Kibens, V., Parekh, D. E., and Glezer, A., "Modification of the Aerodynamics Characteristics of an Unconventional Airfoil Using Synthetic Jet Actuators," *AIAA Journal*, Vol. 39, No. 3, 2001, pp. 361–370.